UKAEA FUS 498

EURATOM/UKAEA Fusion

Confinement of interstitial cluster diffusion by oversized solute atoms

T.S. Hudson, S.L. Dudarev and A.P. Sutton

September 2003

EURATOM/UKAEA Fusion Association

Culham Science Centre
Abingdon
Oxfordshire
OX14 3DB
United Kingdom

Telephone: +44 1235 464181
Facsimile: +44 1235 466435

UKAEA Fusion
Working in Europe

Confinement of interstitial cluster diffusion by oversized solute atoms

By Toby S. Hudson[1], Sergei L. Dudarev[2] and Adrian P. Sutton[1,3]

[1]*Department of Materials, University of Oxford, Parks Road, Oxford OX1 3PH, UK*

[2]*EURATOM/UKAEA Fusion Association, Culham Science Centre, Oxfordshire OX14 3DB, UK*

[3]*Helsinki University of Technology, Laboratory of Computational Engineering, PO Box 9203, FIN-02015 HUT, Finland*

We study the effects of oversized solute atoms on the diffusion of clusters of self-interstitial atoms produced in metals by high energy irradiation. We use kinetic Monte Carlo (KMC) simulations in model BCC iron, and include elastic interactions between the defects. We show that elastic repulsion between solute atoms and the clusters can confine the latter to one dimensional segments. The easy direction of motion of each cluster is assumed to rotate infrequently, allowing it to escape to a new confined segment. The consequences of the confinement for the effective diffusivity of the cluster, and its rate of reaction with other static point defects are explored both by KMC simulations and by an analytic theory. It is shown that the predictions of the theory agree very well with the computer simulations. We suggest some of the possible consequences of these findings for the design of alloys that are more resistant to the effects of high energy radiation damage.

Keywords: Confinement, self-interstitial atom, defect clusters, solute atom, impurity atom, diffusion, transport, kinetic Monte Carlo, radiation damage, computer modelling, dislocation loop, elastic interactions, BCC iron

1. Introduction

The history of our understanding of self-interstitial atom (SIA) clustering and transport has shown the importance of this behaviour to the microstructural evolution of materials irradiated at high energies. 3-D diffusing single SIAs were assumed in *standard rate theory* (SRT) (Brailsford & Bullough 1972, 1981). SRT describes the effects of electron irradiation well. When the *production bias model* (PBM) (Woo *et al.* 1990) was introduced it showed the importance of SIA clustering within the cascade region of high energy radiation damage. However the PBM initially assumed these SIA clusters to be completely sessile objects susceptible to removal only by recombination or 'dislocation sweeping'. Molecular dynamics (MD) simulations then suggested the possibility that in face centered cubic materials, such sessile loops can unfault and become glissile along their glide prism (Foreman *et al.* 1991). This allowed the refinement of the PBM to incorporate 1-D transport, explaining mesoscale structure observed in many situations (Trinkaus *et al.* 1997). Subsequently MD simulations (Bacon *et al.* 1997, 2000; Wirth *et al.* 1997; Osetsky *et al.* 2000a, 2000b) and some experiments (Kiritani 1997; Hayashi *et al.* 2002) have

shown that these glissile clusters can occur in body centred cubic materials as well. Further generalisation of this transport model (Heinisch *et al.* 2000; Trinkaus *et al.* 2002; Golubov *et al.* 2000) has incorporated the importance of the slight non-one-dimensionality of the transport, for example the infrequent rotations of the glide direction onto other close packed axes (Bacon *et al.* 2000; Soneda & Diaz de la Rubia 2001; Doan *et al.* 2001), or conservative climb of clusters diffusing slowly in the plane perpendicular to their fast glide (Hudson *et al.* 2002). Recent KMC simulations incorporating elastic interactions have indicated drastic decreases in long range SIA cluster transport due to 'focusing' in the stress field of a dislocation. In the case of a concentrated system of SIA clusters the focusing is achieved by mutual elastic interactions with other SIA clusters (Ghoniem *et al.* 2002).

This adds up to a substantial body of understanding about the transport of SIAs and their clusters in pure metals. There has long been a belief, and experimental proof that other stress centres such as solute atoms and impurity atoms (in this paper we shall use the terms 'solute' and 'impurity' interchangeably) can influence the evolution of irradiated materials. Examples include the stark differences in irradiated microstructure in nickel alloyed with 2at% of variously sized substitutional solutes (Yoshiie *et al.* 2002), and molecular dynamics simulations of SIA clusters interacting with single vacancies (Pelfort *et al.* 2001) and with oversized copper impurities in BCC iron (Marian *et al.* 2002). The latter study found a decrease in the diffusion prefactor of the cluster, and for small clusters there was an increased frequency of rotations of the Burgers vector. One of the most common methods of describing the effects of impurities, or modelling them in KMC simulations of radiation damage is to consider them as temporary traps for SIA clusters, forming sessile complexes. The complexes may subsequently spontaneously break apart, releasing single interstitials, or the cluster, back into a mobile state. This may be appropriate for some types of solute or impurity atoms (especially undersized) and some temperature conditions, but it does not cover the whole range of possibilitites.

In this paper we describe another transport regime where 1-D confinement of these SIA clusters occurs through repulsive interactions with oversized solute atoms. The clusters can escape from these confined segments only by changing their direction of motion. The 1-D confinement during the period between direction changes can dramatically reduce the effective diffusion coefficient of the SIA cluster. It also reduces the volume of space explored by the cluster over a long period of time, and hence it reduces its rate of reaction with other defects such as vacancy clusters. The region of 3-D space explored by the SIA cluster is more compactly centred on its initial position, because the path lengths between direction changes are no more than the confinement distance. If the confinement distance is small compared to the characteristic microstructural distances in the system, it leads to a transition to behaviour more like the 3-D transport of SRT, even when changes to the direction of motion of the cluster are infrequent. This is a possible origin for the 1-D to 3-D transition assumed in recent explanations of void swelling profiles near grain boundaries formally similar to SRT (Dudarev *et al.* 2003).

Using KMC simulations with elastic interactions described in §2 we demonstrate in §3 that this confinement can occur, and we measure its effect on the diffusion coefficient of SIA clusters and the rates of reaction with static point defects as a function of solute atom concentration. An analytic model is then developed

in §4 for this mode of transport, and compared to these simulation results. The implications of this regime of transport for SIA clusters for microstructural evolution in irradiated materials are discussed in §5.

2. Simulation Methodology

We used the KMC program of (Caturla *et al.* 2000), to which we have added elastic interactions between all defects (Hudson *et al.* 2003), to simulate the motion of SIA clusters in a random distribution of solute atoms in BCC iron.

The interaction between interstitial clusters and oversized impurities was calculated by linear elasticity theory. The interstitial cluster was modelled by a circular perfect dislocation loop with its Burgers vector in a close packed ⟨111⟩ direction perpendicular to the plane of the loop. The direction of easy motion for these clusters is parallel to the Burgers vector of the loop. The energy of interaction between a dislocation loop and an impurity atom, modelled as a centre of dilatation with relaxation volume ΔV, is then $E = \frac{1}{3}(\sigma_{xx} + \sigma_{yy} + \sigma_{zz})\Delta V$, where $(\sigma_{xx} + \sigma_{yy} + \sigma_{zz})$ is the hydrostatic stress generated by the loop at the centre of the point defect.

(*a*) *Elastic Field of a Loop*

Khraishi et al. give an expression for the stress tensor of circular dislocation loops like those we use to model our SIA clusters (Khraishi *et al.* 2001), but this expression has singularities at the circumference of the loop, corresponding to the core of the dislocation. To model the situation where the edge of an interstitial cluster approaches very close to an impurity, we have smoothed out the field near the core of the dislocation in a manner similar to the Peierls-Nabarro model for a straight dislocation (Peierls 1940; Nabarro 1947). This smoothing removes the singularities in the stress field of the loop by introducing a minimum separation, equal to the interatomic distance, between the edge of the loop and the point at which the stress is calculated. Some further modification was required to ensure that stresses near the centre of the loop remain well behaved. Appendix A describes in detail the modified hydrostatic stress field we have used. Figure 1 shows the behaviour in the vicinity of the loop, of the hydrostatic stress as calculated by the smoothed equations (A 3) we have used, compared to that calculated by the original equations of Khraishi *et al.* 2001. In the direction parallel to the axis of the loop, there is recent evidence from atomistic models that elasticity theory underestimates the 'length' of the cluster, in that it has an extended cluster-of-crowdions shape (Puigvi *et al.* 2003). Although this will slightly affect the range at which our interactions become strongly repulsive, it is unlikely to affect our results qualitatively, because the path lengths we consider between solute atoms are far greater than the length of the extended crowdion cluster. It would be impractical to use molecular dynamics simulation for this study, although it might better account for the details of the elastic interactions, because the timescales involved in the rotation of even moderately sized clusters are inaccessible.

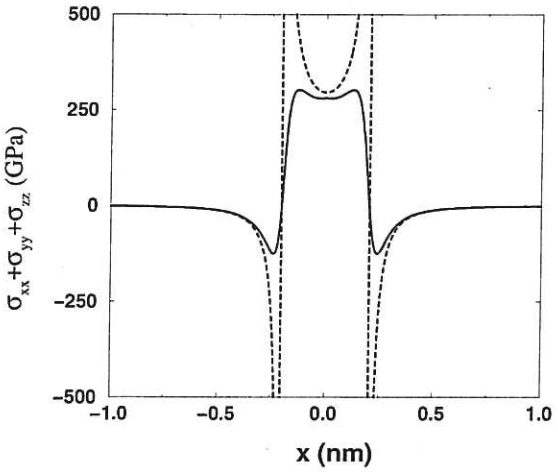

Figure 1. Total hydrostatic stress on a cross section through a 10 interstitial loop (radius 0.22 nm) in BCC iron. Dashed line: according to formulae of Khraishi et. al.; Full line: with smoothing terms as given in Appendix A included to remove singularities.

(*b*) *Configurational Energy Landscape*

For a SIA cluster placed in a randomly distributed field of impurities, figure 2 shows a sample potential energy landscape. We see numerous potential wells, with small potential barriers to entry, where the cluster passes close to an impurity. There are rarer occasions where there is a very large potential barrier, when the loop attempts to go past an impurity located within its glide cylinder. These energy barriers are higher than the depth of the deepest energy wells. This is because all segments of the dislocation loop contribute constructively to the compression within the loop. Outside the loop only nearby segments will contribute tensile stresses, other segments will tend to contribute compressive stresses. The difference between the peak height and the maximum well depth indicates that there is a range of temperature at which loops will be able to pass over all energy wells, but will be able to surmount the energy barriers only very rarely. In this way they may become trapped between pairs of impurities over which effectively they cannot pass. This temperature range will depend on the size of the loop, the relaxation volume of the solute atom, and the host material.

3. KMC results

This section describes our simulations of the characteristic motion of the interstitial cluster in a random field of solute atoms, the effective diffusion coefficient as a function of solute concentration, and the rate of reaction with a third, immobile species.

In all these simulations we have used an interstitial cluster of 10 SIAs, the size of some of the larger clusters formed in 40 keV cascades in BCC iron (Bacon *et al.* 2000), modelled by a circular dislocation loop with radius 0.22 nm, and oversized solute atoms with a relaxation volume of +1.2% of the host atomic volume, and a

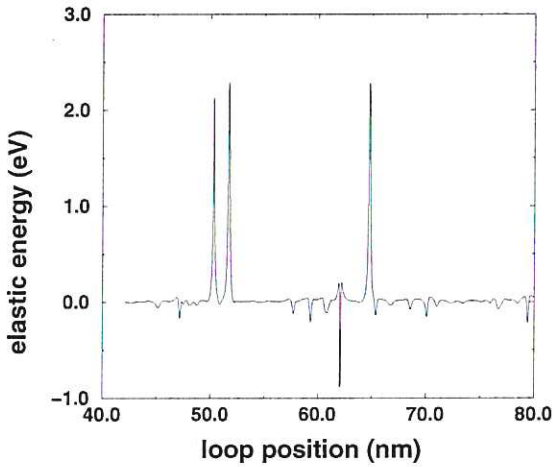

Figure 2. Sample energy landscape for a cluster of 10 self-interstitial atoms in BCC iron, caused by a random field of oversized impurities (formation volume +1.2% of the host atomic volume) at a concentration of 4.0×10^{20} cm^{-3} (corresponding to 0.47 at.%). The cluster is modelled by a circular dislocation loop, and its linear elastic interaction with the impurities is smoothed, as described in the Appendix.

temperature of 1000 K. Under these conditions we expect the confinement between pairs of impurities as described in the previous section. Diffusion is governed by an Arrhenius law $D = \omega_0 a^2 \exp(-E_a/kT)$ with an exponential prefactor of $\omega_0 a^2 = 3.4 \times 10^{-4}$ cm^2 s^{-1}, and an activation energy of $E_a = 0.046$ eV, where ω_0 is the attempt frequency, and a is the diffusive hop length. Rotation to other close packed glide directions is also governed by an Arrhenius law, with an assumed attempt frequency of 0.75×10^{13} s^{-1}, and an assumed activation energy of 1.0 eV. Actual values for these reorientation rates are as yet unknown for such large clusters because the timescale involved is too large for molecular dynamics studies to date. Consequently we restrict ourselves to describing qualitiatively the phenomena involved and do not claim this is a quantitative description of SIA cluster diffusion in BCC iron. The possible dependence of the activation energy of rotation of clusters on the local impurity concentration (Marian *et al.* 2002) is not included in this study, but would further enhance the 3-D nature of the SIA cluster transport in an impurity field.

(*a*) *Confinement*

First we examine the trajectory of a single interstitial cluster through the field of impurities. Figure 3 is a plot of the x, y, and z components of the position of the SIA cluster as a function of time. Because the cluster always travels in a ⟨111⟩ direction, we can detect a rotation of the Burgers vector of this cluster each time the sign of the change in one of these components flips relative to another. The rectangles marked on the figure are positioned to show the times of these Burgers vector changes, and the maximum and minimum extent of the x position component in between rotations. This shows us, that in some cases, for example the

second rectangle, the particle is confined between two points until a rotation occurs, although it is free to diffuse within that segment. In other cases, the endpoints of its confinement are so far apart that it does not explore this length by the time it rotates, e.g. the first box.

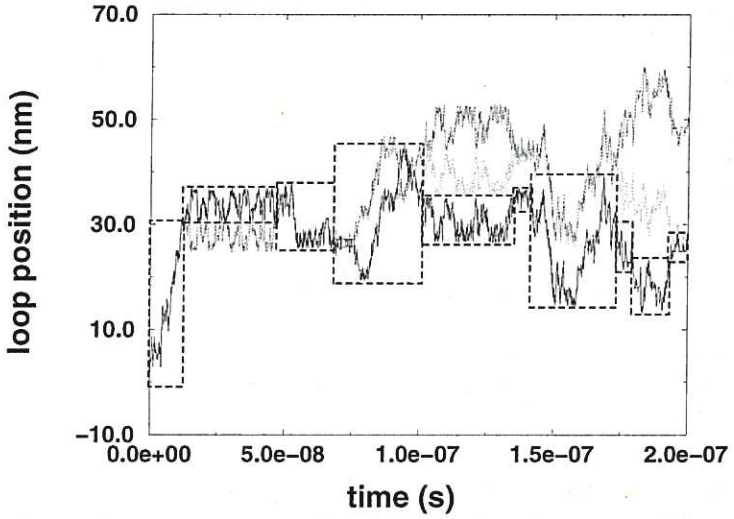

Figure 3. Sample Cartesian trajectory of a cluster of 10 self-interstitial atoms in BCC iron at a temperature of 1000 K, within a field of oversized impurities (formation volume +1.2% of the host atomic volume) at a concentration of 4.0×10^{20} cm^{-3} (corresponding to 0.47 at.%). Initial coordinates: (0, 0, 0). Black: x, dark grey: y, and light grey: z coordinates are plotted against time. Boxes indicate the times of rotations, and the maximum and minimum extent of the x coordinate before the next rotation.

(*b*) *Diffusion*

To measure the effect of this confinement by impurites on the overall transport, we simulated motion of SIA clusters to obtain numerous trajectories, each over a time of 2×10^{-7} s , from which mean squared displacements and effective diffusion coefficients could be extracted. These effective diffusion coefficients are plotted as a function of impurity concentration in figure 4. They are compared to results of an analytical model, equation (4.12), which will be described below. Both show an initial insensitivity to impurities, when the concentration of impurities is so low that collisions with them are infrequent. At larger concentrations where confinement can occur within the typical distance between Burgers vector rotations, a drastic decrease in the diffusion coefficient occurs with increasing concentration.

(*c*) *Reaction*

The confinement by impurities also has a substantial effect on any reactions involving the interstitial clusters. Simulations were performed of an SIA cluster in a randomly distributed field of stationary spherical sinks with no elastic field.

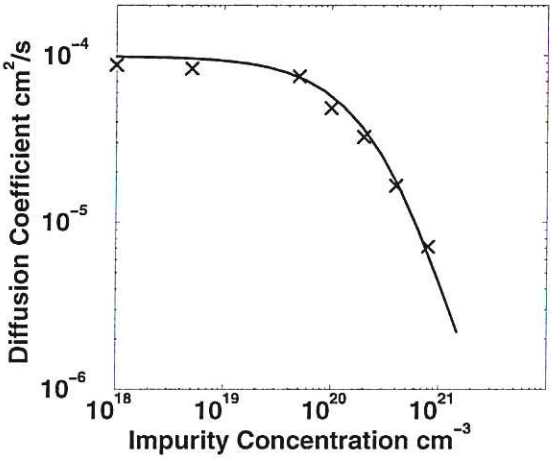

Figure 4. Effective diffusion coefficient for a 10 SIA cluster in BCC iron undergoing 1-D diffusion with rare direction changes at a temperature of 1000 K, within a field of oversized impurities (formation volume +1.2% of the host atomic volume), as a function of impurity concentration. Crosses: KMC results. Line: As predicted by model in section §4 *a*.

The concentration of these sinks was 1×10^{19} cm^{-3}, and the capture radius used was 0.68 nm. Each sink is assumed to be a perfect absorber. We compare the case of annihilation in a pure material to the case of annihilation in a random field of stationary solute atoms with a concentration of 4×10^{20} cm^{-3}. Many simulations of annihilations of individual SIA clusters were performed in this manner, 10 000 in pure iron and 200 in impure iron, to determine the probability of a cluster surviving in the presence of these sinks as a function of time. These probabilities are plotted and compared to theoretical curves from equations (4.30) and (4.14) in figure 5. It is seen that the probability of survival of an SIA cluster is enhanced considerably, especially at longer times, when solute atoms are present that confine the 1-D diffusion of the SIA cluster. More generally, we conclude that oversized solute atoms will reduce the rates of reaction between SIA clusters and static defect clusters, such as vacancy clusters.

4. Theoretical Analysis

In this section we present an analytic model system that enables us to generalize the results of the KMC simulations described in §3. To understand the behaviour of the loops in the stress fields caused by the impurity atoms, we construct the following model system, for comparison to the KMC results in §3. Consider a temperature where loops are freely able to pass over the energy wells arising from attractive interactions to impurities nearby, but where loops are unable to overcome the large energy barriers provided by direct traversals of an impurity atom. In this case, until the Burgers vector of the loop rotates, we treat the transport as 1-D Brownian motion except that it is limited by the fact that it is always reflected when it encounters an impurity directly.

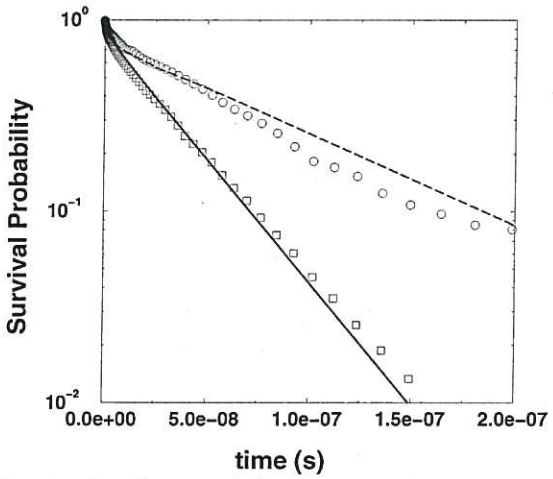

Figure 5. Survival probability for a 10 SIA cluster undergoing 1-D diffusion with rare direction changes at a temperature of 1000 K, in a field of spherical sinks (Concentration: 1×10^{19} cm^{-3}, capture radius 0.68 nm) without an elastic field, plotted against time. Squares: KMC results in pure BCC iron; Circles: KMC results with an oversized impurity (formation volume +1.2% of the host atomic volume) concentration of 4×10^{20} cm^{-3}. Curves: as predicted by model in §4 *b*, full: in a pure material, dashed: with oversized impurity field.

Confinement will dramatically alter both the overall distance loops can diffuse in a given time and the volume of space they explore. Since interstitial clusters generally diffuse much faster than other species in the system, the volume they explore as a function of time is very important to rates of reaction with other defects. In §4 *a* we focus on estimating the effective diffusion coefficient in the presence of confinement, as a function of the diffusion coefficient of the SIA cluster in a pure material, the solute concentration, and the frequency of rotations of the Burgers vector. In §4 *b* we will investigate analytically the reaction rates with a field of small spherical stationary sinks. These analytic results are compared with the simulations described in §3.

(*a*) *Effective diffusion coefficient*

(i) *Confined 1-D motion*

For one dimensional diffusion of a loop along the x-axis, confined to a 'box' between $x = 0$ and $x = L$, and starting at position x_0 within the box, the probability distribution for the location of the loop after time t is given by:

$$p(x,t) = \frac{1}{L} + \frac{2}{L}\sum_{n=1}^{\infty} \cos\left(\frac{n\pi x_0}{L}\right) \cos\left(\frac{n\pi x}{L}\right) \exp\left(-\frac{n^2\pi^2 Dt}{L^2}\right) \qquad (4.1)$$

To obtain an effective diffusion coefficient, the first quantity required is the mean squared displacement as a function of time while the loop remains confined in this box. The initial position x_0 within the box is selected from a uniform distribution

(see discussion of equation (4.4)), so we will average over all possible x_0. We denote this mean squared displacement $g(L,t)$:

$$\begin{aligned} g(L,t) &= \frac{1}{L^2}\int_0^L \int_0^L p(x,t)\,(x-x_0)^2\,dx dx_0 \\ &= \frac{L^2}{6} - \frac{16L^2}{\pi^4}\sum_{n=0}^{\infty} \frac{\exp\left(-\dfrac{(2n+1)^2\pi^2 Dt}{L^2}\right)}{(2n+1)^4} \end{aligned} \tag{4.2}$$

Assuming the impurities in the material are distributed at random, there will be a distribution of lengths of confinement. If $P_l(L)$ is the distribution of lengths to the left of our initial starting point before we reach an impurity, and $P_r(L)$ is the same distribution to the right, then we have:

$$P_l(L) = P_r(L) = \frac{\exp\left(-\frac{L}{L_0/2}\right)}{L_0/2} \tag{4.3}$$

where $L_0 = 2/(\pi r^2 N)$ is the mean distance between impurities, r is the radius of the loop, N is the concentration of impurities. This means that the overall box length distribution is:

$$\begin{aligned} P(L) &= \int_0^L P_l(L-y)\,P_r(y)\,dy \\ &= \int_0^L \frac{4\exp(-\frac{L}{L_0/2})}{L_0^2}dy \\ &= \frac{4L\exp(-\frac{L}{L_0/2})}{L_0^2} \end{aligned} \tag{4.4}$$

Note that in the last step the integrand was independent of y, implying that the ensemble of clusters which are initially confined in a particular boxlength L will initially be spread uniformly, justifying our use of the particular average in equation (4.2).

It follows from equations (4.2) and (4.4) that the mean squared displacement for a 1-D diffusing cluster positioned at random in this impurity field is:

$$\bar{g}(t) = \frac{4}{L_0^2}\int_0^{\infty} g(L,t)\,L\exp\left(-\frac{2L}{L_0}\right)dL \tag{4.5}$$

The lowermost curve in figure 6 shows this function for a concentration of impurities corresponding to an average boxlength of $L_0 = 32$ nm where the initial gradient is equivalent to diffusion in a pure medium, with diffusion coefficient of $D = 10^{-4}$ cm^2 s^{-1}.

(ii) *Confined 1-D motion with rotations*

Now we examine the case where random infrequent rotations are introduced. Because they are not correlated, the probability $R_n(\tau)$ of having undergone

rotations of the Burgers vector exactly n times after the system has evolved for time τ is given by the Poisson distribution:

$$R_n(\tau) = \frac{\tau^n \exp\left(-\frac{\tau}{t^*}\right)}{n!(t^*)^n} \tag{4.6}$$

where t^* is the average time between rotations.

We can find the fraction $j_{n+1}(t,\tau)$ of all the particles, which have made $n+1$ rotations after time τ and have lived in that $n+1$ state for a time t. Clearly $j_{n+1}(t,\tau) = 0$ for $t > \tau$, so the interesting distribution is for $t < \tau$. Also, $j_0(t,\tau)$ is special because a loop that has never rotated must have been in that same state as long as the system has been evolving. Thus we have:

$$j_0(t,\tau) = R_0(\tau)\,\delta(\tau - t) \tag{4.7}$$

For one or more rotations we have:

$$j_{n+1}(t,\tau) = R_n(\tau - t)\,\frac{1}{t^*}\exp\left(-\frac{t}{t^*}\right) \text{ for } t < \tau \tag{4.8}$$

which is the fraction R_n that were able to convert to state $n+1$ at time $\tau - t$, multiplied by the rate of conversion $1/t^*$, multiplied by the probability of survival in this state for time t, $\exp(-t/t^*)$.

We now make the approximation that each time a rotation occurs, a new pair of impurity endpoints is chosen, that has never been sampled before, i.e. the cluster never returns to a confinement segment it occupied earlier. This is likely to be valid when the impurities are single atoms, and the average path length is much larger than the radius of the loop. In that case, the mean squared displacement it undergoes from its new starting point along the new confined segment can simply be added to the total mean squared displacement for its entire journey.

We define $h(\tau)$ as the mean squared displacement after a time τ from the initial position of a loop randomly inserted in the impure crystal.

$$\frac{dh(\tau)}{d\tau} = \sum_{n=0}^{\infty}\int_0^{\tau} j_n(t,\tau)\,\frac{d\bar{g}(t)}{dt}dt \tag{4.9}$$

This general form for the rate of increase of the mean squared displacement may be explained as follows. For a given number of rotations we multiply the probability distribution function for the SIA cluster being confined for a time t in its current confinement segment, given that the total elapsed time is τ, by the rate of increase of mean squared displacement we would expect after being confined for this time t. We integrate this product over all confinement times and sum over all numbers of rotations.

Combining equations (4.6), (4.7), (4.8) and (4.9), we get:

$$\begin{aligned}\frac{dh(\tau)}{d\tau} &= \exp\left(-\frac{\tau}{t^*}\right)\frac{d\bar{g}(\tau)}{d\tau} + \\ &\sum_{n=1}^{\infty}\int_0^{\tau}\frac{1}{(n-1)!}\left(\frac{\tau - t}{t^*}\right)^{n-1}\frac{1}{t^*}\exp\left(-\frac{\tau}{t^*}\right)\frac{d\bar{g}(t)}{dt}dt\end{aligned} \tag{4.10}$$

which can be simplified to:

$$\frac{dh(\tau)}{d\tau} = \exp\left(-\frac{\tau}{t^*}\right)\frac{d\bar{g}(\tau)}{d\tau} + \frac{1}{t^*}\int_0^{\tau}\exp\left(-\frac{t}{t^*}\right)\frac{d\bar{g}(t)}{dt}dt \tag{4.11}$$

To illustrate the range of possible behaviour predicted by equation (4.11) we show in figure 6 the limit of the equation in a pure material ($L_0 \to \infty$), which corresponds to free diffusion. We integrate equation (4.11) numerically, with the initial condition $h(0) = 0$, and also show the case of complete 1-D confinement by a randomly distributed field of solute atoms when no rotations are allowed, and finally two intermediate cases with the same confinement length distribution but with rotations allowed.

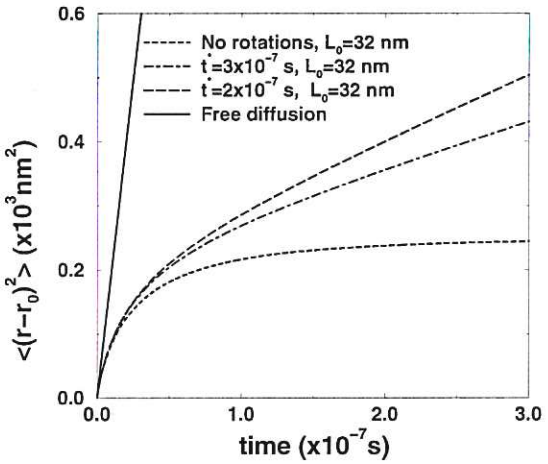

Figure 6. Representative cases of the theoretical mean squared displacement as a function of time. t^* is the mean time between rotations, L_0 is the mean confinement length. 4 cases are shown: free diffusion; 1-D confinement with $L_0 = 32$ nm; confinement where $L_0 = 32$ nm but rotations are allowed: with $t^* = 3 \times 10^{-7}$ s; and with $t^* = 2 \times 10^{-7}$ s. All cases use $D = 10^{-4}$ cm^2 s^{-1}.

To obtain effective diffusion coefficients at long times, corresponding to linear parts of the curves in figure 6, we take the limit $\tau \to \infty$ and recalling that $\bar{g}(0) = 0$, we get:

$$\left.\frac{dh(\tau)}{d\tau}\right|_{\tau=\infty} = \frac{1}{t^{*2}}\int_0^{\infty}\exp\left(-\frac{t}{t^*}\right)\bar{g}(t)\,dt \tag{4.12}$$

When the lengths of paths between rotations are small compared to the mean distance between impurities, equation (4.12) reduces to the same diffusive behaviour as the loop would undergo in a pure crystal

$$D_{eff} = \frac{1}{6}\left.\frac{dh(\tau)}{d\tau}\right|_{\tau=\infty} \approx \frac{D}{3}$$

The factor of 3 comes from the fact that we have 'bent' 1D motion into 3 dimensions. The opposite limit where rotations are rare and the impurity concentrations are significant, results in an effective diffusion coefficient:

$$D_{eff} = \frac{1}{6}\left.\frac{dh(\tau)}{d\tau}\right|_{\tau=\infty} \approx \frac{L_0^2}{24t^*} = \frac{1}{6\left(\pi r^2 N\right)^2 t^*}$$

Note that in this limit the effective diffusion coefficient is independent of the coefficient D of *one-dimensional diffusion* and is inversely proportional to the square of the concentration of solute atoms N in the material as well as to the square of the number ν of SIAs forming the cluster $\nu \sim \pi r^2$.

(b) *Effective reaction rates*

We now consider the effective capture rate of a SIA cluster diffusing as above in a randomly distributed field of impurities, and in the presence of perfectly absorbing stationary spherical sinks with a capture radius of r_c. We let $[I(\tau)]$ and $[S]$ be the concentrations of interstitial clusters and sinks respectively, and $Z(\tau)$ be the total length of the path through the material traversed by the cluster at least once, as a function of time τ.

$$\frac{d[I(\tau)]}{d\tau} = -[I(\tau)][S]\pi r_c^2 \frac{dZ(\tau)}{d\tau} \tag{4.13}$$

So the survival probability at time τ is:

$$f = \frac{[I(\tau)]}{[I(0)]} = \exp\left(-[S]\pi r_c^2 Z(\tau)\right) \tag{4.14}$$

The key parameter that impurities will affect is $Z(\tau)$, and we will now derive an expression for it.

(i) *Free 1-D exploration*

Consider an unconfined 1-D random walk, comprising random hops $X_1, X_2, \ldots$ where $X_i = \pm 1$. Define the currect position Y_n, the maximum to date M_n^+, and minimum to date M_n^-:

$$\begin{aligned} Y_n &= X_1 + X_2 + \ldots + X_n \\ M_n^+ &= \max(Y_1, Y_2, \ldots Y_n) \\ M_n^- &= \min(Y_1, Y_2, \ldots Y_n) \end{aligned} \tag{4.15}$$

Using the *reflection principle*, it has been shown that (see for example http://www.math.uah.edu/statold/walk/walk2.html):

$$\begin{aligned} P\left(M_n^+ = m\right) &= P\left(Y_n = m\right) \qquad \text{when } m \bmod 2 = n \bmod 2 \\ P\left(M_n^+ = m\right) &= P\left(Y_n = m+1\right) \qquad \text{when } m \bmod 2 \neq n \bmod 2 \end{aligned} \tag{4.16}$$

As n increases the combinatorial solution for the distribution Y_n can be approximated by exponential terms using Stirling's rule. We also replace the discrete variables, the number n of hops and the current position $Y_n = m$,

with continous variables time t and current position $Y = x$. The density of our probability distribution function $P(M^+ = x, t)$ approaches double the density of the probability distribution function $P(Y = x, t)$, because the discrete probability distribution $P(Y_n = m)$ is 0 when n and m are of different parity.

The continuous description of the distribution $P(Y = x, t)$ is the well known case of Brownian motion:

$$P(Y = x, t) = \frac{1}{2(\pi D t)^{\frac{1}{2}}} \exp\left(-\frac{x^2}{4Dt}\right) \tag{4.17}$$

It follows that the distribution of maximal values of 1-D Brownian motion after time t is:

$$P\left(M^+ = x, t\right) = \frac{1}{(\pi D t)^{\frac{1}{2}}} \exp\left(-\frac{x^2}{4Dt}\right) \text{ for } x > 0 \tag{4.18}$$

By symmetry the distribution of minimal values of a 1-D Brownian walk after time t is:

$$P\left(M^- = -x, t\right) = P\left(M^+ = x, t\right) \tag{4.19}$$

To calculate the average distance explored in the positive direction as a function of time, we evaluate:

$$\begin{aligned} \langle M^+(t) \rangle &= \int_0^\infty x \frac{1}{(\pi D t)^{\frac{1}{2}}} \exp\left(-\frac{x^2}{4Dt}\right) dx \\ &= 2\left(\frac{Dt}{\pi}\right)^{\frac{1}{2}} \end{aligned} \tag{4.20}$$

Using the symmetry between the minimal value distribution and the maximal value distribution, we get the average total distance explored in both directions as a function of time:

$$\langle M^+(t) - M^-(t) \rangle = 4\left(\frac{Dt}{\pi}\right)^{\frac{1}{2}} \tag{4.21}$$

(ii) *Confined 1-D exploration*

We consider how the average total distance explored of equation (4.21) changes when we confine the cluster between impenetrable objects distance L apart. Initially mimicking the above behaviour, the explored distance will eventually saturate at L.

To evaluate the explored distance, we first go back to the free case, and consider the probability that a 1-D diffusing particle starting at the origin does not leave the interval $(-x_L, x_H)$ in time t: $P(x_L, x_H, t) = P((M^- \geq -x_L) \ \& \ (M^+ \leq x_H), t)$. This probability can be evaluated in three steps. First by solving the diffusion equation in this interval with the boundary conditions that at both ends the concentration is fixed at 0, equivalent to absorbing walls, we obtain the distribution of positions of particles which have remained between these bounds. Secondly, this solution is integrated over this interval to find the fraction of the diffusing particles

that have remained always in this interval.

$$P(x_L, x_H, t) = \frac{4}{\pi} \sum_{m=0}^{\infty} \frac{\sin\left(\frac{(2m+1)\pi x_L}{x_L + x_H}\right)}{2m+1} \exp\left(-\frac{(2m+1)^2 \pi^2 Dt}{(x_L + x_H)^2}\right) \quad (4.22)$$

In the third step, we follow Berezhkovskii *et al.* 1989, and find the joint probability distribution of the Brownian trajectory for which the maximal deviations of the centre of the cluster during time t to the left and right of the starting point are exactly x_L and x_H respectively (their equation (32)):

$$\Psi(x_L, x_H, t) = \frac{\partial^2 P(x_L, x_H, t)}{\partial x_L \partial x_H} \quad (4.23)$$

We note that our equation for $P(x_L, x_H, t)$ in 4.22 differs significantly from the equivalent equation given in Berezhkovskii *et al.* 1989, although we have followed their method. Using our expression we get:

$$\begin{aligned}
&\Psi(x_L, x_H, t) = \\
&\frac{4}{\pi} \sum_{m=0}^{\infty} \left\{ \left[B\left(x_L^2 - x_H^2\right) \left(-2C + (x_L + x_H)^2\right) \cos\left(\frac{Bx_L}{x_L + x_H}\right) + \right.\right. \\
&\left.\left(4C^2 - 6C(x_L + x_H)^2 + B^2 x_L x_H (x_L + x_H)^2\right) \sin\left(\frac{Bx_L}{x_L + x_H}\right) \right] \times \\
&\left.\left((2m+1) \exp\left(\frac{C}{(x_L + x_H)^2}\right) (x_L + x_H)^6\right)^{-1} \right\}
\end{aligned} \quad (4.24)$$

where

$$\begin{aligned}
B &= (2m+1)\pi \\
C &= (2m+1)^2 \pi^2 Dt
\end{aligned}$$

Because a particle must have exactly one maximal deviation on either side of its origin, the identity $\int_0^\infty dx_L \int_0^\infty dx_H \Psi(x_L, x_H, t) = 1$ must hold.

Using $\Psi(x_L, x_H, t)$, we now consider the case of a particle constrained within a box of length $L = l_1 + l_2$. The particle starts at the origin, which is l_1 to the right of the left of the box. Let $z(l_1, l_2, t)$ be the average distance explored after time t. It is obtained by folding the joint probability distribution for a free particle, shown in equation (4.24), at both ends of the box. For example if a free particle trajectory folded over from the right hand end of the box overlaps so far that it covers the left hand side of the box, then irrespective of the maximal excursion on the left hand side, the whole box length has been explored. Averaging over all trajectories, the expected length explored after time t, having started at position l_1 from the left of the box, is:

$$z(l_1, l_2, t) = \int_0^\infty dx_L \int_0^\infty dx_H \Psi(x_L, x_H, t) \left[\begin{array}{l} \max(x_H, x_L - 2l_1, l_2) + \\ \max(x_L, x_H - 2l_2, l_1) \end{array} \right] \quad (4.25)$$

We can break these integrals into segments:

$$
\begin{aligned}
& z\left(l_1, l_2, t\right) = \\
& \int_{2l_1+l_2}^{\infty} dx_L \left[\begin{array}{l} \int_0^{l_2} dx_H \Psi\left(x_L, x_H, t\right)[L] + \\ \int_{l_2}^{\infty} dx_H \Psi\left(x_L, x_H, t\right)[L] \end{array} \right] + \\
& \int_{2l_1}^{2l_1+l_2} dx_L \left[\begin{array}{l} \int_0^{l_2} dx_H \Psi\left(x_L, x_H, t\right)[l_1 + \max\left(-2l_1 + x_L, x_H\right)] + \\ \int_{l_2}^{\infty} dx_H \Psi\left(x_L, x_H, t\right)[L] \end{array} \right] + \\
& \int_{l_1}^{2l_1} dx_L \left[\begin{array}{l} \int_0^{l_2} dx_H \Psi\left(x_L, x_H, t\right)[l_1 + x_H] + \\ \int_{l_2}^{\infty} dx_H \Psi\left(x_L, x_H, t\right)[L] \end{array} \right] + \\
& \int_0^{l_1} dx_L \left[\begin{array}{l} \int_0^{l_2} dx_H \Psi\left(x_L, x_H, t\right)[x_L + x_H] + \\ \int_{l_2}^{2l_2} dx_H \Psi\left(x_L, x_H, t\right)[x_L + l_2] + \\ \int_{2l_2}^{2l_2+l_1} dx_H \Psi\left(x_L, x_H, t\right)[\max\left(x_L, x_H - 2l_2\right) + l_2] + \\ \int_{2l_2+l_1}^{\infty} dx_H \Psi\left(x_L, x_H, t\right)[L] \end{array} \right]
\end{aligned}
\tag{4.26}
$$

Grouping together the three terms which involve the integral over x_H from l_2 to ∞ we obtain the first line of the following equation, and the remaining terms are simplifications of the corresponding integrals in equation (4.26):

$$
\begin{aligned}
z\left(l_1, l_2, t\right) &= L \times P\left(\left(M^- \leq -l_1\right) \,\&\, \left(M^+ \geq l_2\right)\right) \\
&+ L \times P\left(\left(M^- \leq -l_2 - 2l_1\right) \,\&\, \left(M^+ \leq l_2\right)\right) \\
&+ \int_{2l_1}^{l_2+2l_1} dx_L \int_0^{l_2} dx_H \left[l_1 + \max\left(x_H, -2l_1 + x_L\right)\right] \Psi\left(x_L, x_H, t\right) \\
&+ \int_{l_1}^{2l_1} dx_L \int_0^{l_2} dx_H \left(x_H + l_1\right) \Psi\left(x_L, x_H, t\right) \\
&+ \int_0^{l_1} dx_L \int_0^{l_2} dx_H \left(x_H + x_L\right) \Psi\left(x_L, x_H, t\right) \\
&+ \int_0^{l_1} dx_L \int_{l_2}^{2l_2} dx_H \left(l_2 + x_L\right) \Psi\left(x_L, x_H, t\right) \\
&+ \int_0^{l_1} dx_L \int_{2l_2}^{2l_2+l_1} dx_H \left[l_2 + \max\left(x_L, x_H - 2l_1\right)\right] \Psi\left(x_L, x_H, t\right) \\
&+ L \times P\left(\left(M^- \geq -l_1\right) \,\&\, \left(M^+ \geq 2l_2 + l_1\right)\right)
\end{aligned}
\tag{4.27}
$$

The next step is to average $z\left(l_1, l_2, t\right)$ over all possible initial positions in the box to get $\bar{z}\left(L, t\right)$:

$$
\bar{z}\left(L, t\right) = \frac{1}{L} \int_0^L z\left(l_1, L - l_1, t\right) dl_1 \tag{4.28}
$$

The final step is to average $\bar{z}\left(L, t\right)$, over the box length distribution as in equation (4.5) to get $\bar{\bar{z}}\left(t\right)$ for a given solute atom concentration:

$$
\bar{\bar{z}}\left(t\right) = \frac{4}{L_0^2} \int_0^{\infty} \bar{z}\left(L, t\right) L \exp\left(-\frac{2L}{L_0}\right) dL \tag{4.29}
$$

(iii) *Confined 1-D exploration with rotations*

With $\bar{\bar{z}}(t)$, we can use similar arguments to that used in equation (4.11) to get the average total volume explored as a function of time τ:

$$\frac{dZ(\tau)}{d\tau} = \exp\left(-\frac{\tau}{t^*}\right)\frac{d\bar{\bar{z}}(\tau)}{d\tau} + \frac{1}{t^*}\int_0^\tau \exp\left(-\frac{t}{t^*}\right)\frac{d\bar{\bar{z}}(t)}{dt}dt \qquad (4.30)$$

Note that we have not squared the total length explored at any stage here as we did in the analysis in §4 *a*. The reason is that when a cluster changes directions and starts a new confined exploration, the new explored distance itself additively contributes to the mean total length explored. In §4 *a* however, it was the squares of the new displacements which additively contributed to the total mean squared displacement. Our assumption of additive contributions to the mean total length explored requires long lengths for each 1-D path compared to the cluster radius. In the case of very high impurity concentrations, or very frequent rotations, this approximation breaks down and 3D volume exploration models should be used.

Now that we have an expression for Z, then rates of reaction with stationary sinks may be obtained as discussed in equation (4.14). The results compare favourably to the KMC simulations, as shown in figure 5.

5. Implications and Conclusions

We have argued in this paper that under certain conditions of temperature, frequency of rotation of SIA clusters, and concentration of solute atoms, the diffusivity of these clusters, and their ability to reach and react with other defects, may be severely curtailed by oversized solute atoms confining their one-dimensional excursions. Undersized impurities or oversized impurities at low temperatures may attract and trap SIA clusters. At higher temperatures we expect confinement by repulsion from oversized impurities at either end of a 1-D segment along which there is otherwise free diffusion. We have observed this confinement in the kinetic Monte Carlo simulations of §3. Rotation of the Burgers vector eventually allows the SIA clusters to migrate over greater distances, but the effective diffusion coefficient and the rate of volume exploration can be much lower than that of a cluster diffusing freely in a pure material. The confinement to short segments accompanied by rotations of the Burgers vector destroys the long ballistic motion characteristic of typical 1-D transport of these interstitial clusters, making the diffusion effectively 3-D on a smaller spatial scale. This is possible even for clusters which rotate only very infrequently and would in a pure material be considered to have near 1-D transport. Near 3-D motion of the clusters in such alloys may render void explanations of the observed larger-scale microstructural features that rely on near 1-D transport.

An analytic theory is presented in §4 and compared to the KMC simulation results. It successfully accounts for both the reduction in effective diffusion coefficient, and the reduction in reaction rates associated with a reduced ability to explore space found in the KMC simulations.

The partially confined motion of SIA clusters able to undergo Burgers vector rotations presents further questions about how the impurity interaction affects the evolution of a high-energy radiation cascade in alloys. Because the SIA clusters will remain in the vicinity of where they were created for longer, near the vacancies and

vacancy clusters, and because they will explore more 3-dimensionally in that region, we expect higher levels of recombination within the cascade after the thermal spike. More generally, it should be possible to tailor the solute composition in reactor materials to take advantage of their reduction of the transport of SIA clusters, to design alloys resistant to high-energy radiation damage, for example enhancing recombination and thereby reducing swelling.

This work was supported by the UK Office of Science and Technology, Engineering and Physical Sciences Research Council, EURATOM, the Overseas Research Students Award Scheme, and a Linacre College Applied Materials Scholarship. The authors wish to thank Georges Martin for helpful discussions. The authors also wish to thank Maria-José Caturla for the provision of the bigmac computer program, and subsequent instructive discussions.

Appendix A. Equations for hydrostatic stress from loops

The equations according to Khraishi *et. al.* 2001 for the uniaxial stress components of a circular dislocation loop with Burgers vector in the z direction perpendicular to the habit plane of the loop are:

$$\begin{aligned} \sigma_{xx} &= C\left[D_9E(k)+D_{10}K(k)\right]+C'\left[D_{11}E(k)+D_{12}K(k)\right] \\ \sigma_{zz} &= C'\left[D_3E(k)+D_4K(k)\right] \end{aligned} \tag{A 1}$$

where $K(k)$ is the complete elliptic integral of the first kind, and $E(k)$ is the complete elliptic integral of the second kind, and the coefficients D_3, D_4, D_9, D_{10}, D_{11}, and D_{12} are functions of the variables:

$$\begin{aligned} \rho &= \left(x^2+y^2\right)^{\frac{1}{2}} \\ r &= \left(\rho^2+z^2\right)^{\frac{1}{2}} \\ C &= -\frac{Gb_z}{\pi} \\ C' &= \frac{Gb_z}{2\pi(1-\nu)} \\ a &= r^2+R^2 \\ b &= 2\rho R \\ k &= \left(\frac{2b}{a+b}\right)^{\frac{1}{2}} \end{aligned} \tag{A 2}$$

The expression for σ_{yy} can be obtained from the expression for σ_{xx} by switching x and y.

The expressions we have used for the coefficients D_3, D_4, D_9, D_{10}, D_{11}, and D_{12}, are given in equation (A 3). We have followed the notation of Khraishi *et. al.* 2001. These coefficients have been smoothed by addition of the term A^2, a constant the size of the interatomic distance squared, each time the term $a-b=z^2+(R-\rho)^2$ was required, to remove the stress singularities at the location of the dislocation core. For very small loops such as the loop modelled here, a smaller constant $A \sim R/10$ is required to eliminate the divergent behaviour. D_{12} is also multiplied by the factor $(a-b)/(a-b+A^2)$ to correct for a singularity which otherwise appears in the centre of the loop. This factor approaches 1 when far from the loop.

$$
\begin{aligned}
D_3 &= \frac{(a+b)(a-b+A^2)(a-2R^2)+z^2(a^2+3b^2)-8az^2R^2}{(a-b+A^2)^2(a+b)^{\frac{3}{2}}} \\
D_4 &= \frac{-(a-b+A^2)(a+b)-z^2(a-2R^2)}{(a-b+A^2)(a+b)^{\frac{3}{2}}} \\
D_9 &= \frac{((a-b+A^2)(a+b)(y^2-x^2)-y^2\rho^2(a-2R^2))}{(a-b+A^2)(a+b)^{\frac{1}{2}}\rho^4} \\
D_{10} &= \frac{a(x^2-y^2)+y^2\rho^2}{(a+b)^{\frac{1}{2}}\rho^4} \\
D_{11} &= \frac{\left(\begin{array}{l} a(a-b+A^2)(a+b)(x^2-y^2)R^2+ \\ \{(a-b+A^2)(a+b)\left[2(a-3R^2)x^2+ay^2\right]- \\ (a^2+3b^2-8aR^2)x^2z^2\}\rho^2 \end{array}\right)}{(a-b+A^2)^2(a+b)^{\frac{3}{2}}\rho^4} \\
D_{12} &= \frac{a-b}{a-b+A^2}\times\frac{\left(\begin{array}{l} (a-b+A^2)(a+b)(y^2-x^2)R^2- \\ \left[(a-b+A^2)(a+b)(2x^2+y^2)-(a-2R^2)x^2z^2\right]\rho^2 \end{array}\right)}{(a-b+A^2)(a+b)^{\frac{3}{2}}\rho^4}
\end{aligned}
\tag{A 3}
$$

References

Bacon, D. J., Calder, A. F. & Gao, F. 1997 Defect production due to displacement cascades in metals as revealed by computer simulation. *J. Nucl. Mater.* **251**, 1–12.

Bacon, D. J., Gao, F. & Osetsky Yu. N. 2000 The primary damage state in fcc, bcc and hcp metals as seen in molecular dynamics simulations. *J. Nucl. Mater.* **276**, 1–12.

Berezhkovskii, A. M., Makhnovskii, Yu. A. & Suris, R. A. 1989 Wiener sausage volume moments. *J. Stat. Phys.* **57**, 333–346.

Brailsford, A. D. & Bullough, R. 1972 The rate theory of swelling due to void growth in irradiated materials. *J. Nucl. Mater.* **44**, 121–135.

Brailsford, A. D. & Bullough, R. 1981 The theory of sink strengths. *Phil. Trans. R. Soc. Lond.* **302**, 87–136.

Caturla, M. J., Soneda, N., Alonso, E., Wirth, B. D., Diaz de la Rubia, T. & Perlado, J. M. 2000 Comparative study of radiation damage accumulation in Cu and Fe. *J. Nucl. Mater.* **276**, 13–21.

Doan, N. V., Rodney, D. & Martin, G. 2001 Interstitial cluster motion in nickel: a molecular dynamics study. *Defect and Diffusion Forum* **194–199**, 43–48.

Dudarev, S. L., Semenov, A. A. & Woo, C. H. 2003 Heterogeneous void swelling near grain boundaries in irradiated materials. *Phys. Rev.* B **67**, art. no. 094103.

Foreman, A. J. E., English, C. A. & Phythian, W. J. 1991 *A. E. A. Technology Harwell Rept.* AEA-TRS-2028 and 2031.

Ghoniem, N. M., Tong, S. H., Huang, J., Singh, B. N. & Wen, M. 2002 Mechanisms of dislocation-defect interactions in irradiated materials investigated by computer simulations. *J. Nucl. Mater.* **307–311**, 843–851.

Golubov, S. I., Singh, B. N. & Trinkaus, H. 2000 Defect accumulation in fcc and bcc metals and alloys under cascade damage conditions - towards a generalisation of the production bias model. *J. Nucl. Mater.* **276**, 78–89.

Hayashi, T., Fukmuto, K. & Matsui, H. 2002 In situ observation of glide motions of SIA-type loops in vanadium and V-5Ti under HVEM irradiation. *J. Nucl. Mater.* **307–311**, 993–997.

Heinisch, H. L., Singh, B. N. & Golubov S. I. 2000 The effects of one-dimensional glide on the reaction kinetics of interstitial clusters. *J. Nucl. Mater.* **283-287**, 737-740.

Hudson, T. S., Dudarev, S. L. & Sutton, A. P. 2002 Absence of saturation of void growth in rate theory with anisotropic diffusion. *J. Nucl. Mater.* **307–311**, 976–981.

Hudson, T. S., Dudarev, S. L., Caturla, M. J. & Sutton, A. P. Effects of elastic interactions on post-cascade radiation damage evolution in kinetic Monte-Carlo simulations. (In press).

Kiritani, M. 1997 Defect interaction processes controlling the accumulation of defects produced by high energy recoils. *J. Nucl. Mater.* **251**, 237–251.

Khraishi, T. A., Zbib, H. M., Diaz de la Rubia, T. & Victoria, M. 2001 Modelling of irradiation-induced hardening in metals using dislocation dynamics. *Phil. Mag. Lett.* **81**, 583–593.

Marian, J., Wirth, B. D., Caro, A., Sadigh, B., Odette, G. R., Perlado, J. M. & Diaz de la Rubia, T. 2002 Dynamics of self-interstitial cluster migration in pure α-iron and Fe-Cu alloys. *Phys. Rev.* B **65**, art. no. 144 102.

Nabarro, F. R. N. 1947 Dislocations in a simple cubic lattice. *Proc. Phys. Soc.* **59**, 256–272.

Osetsky, Yu. N., Serra, A., Singh, B. N. & Golubov, S. I. 2000*a* Structure and properties of clusters of self-interstitial atoms in fcc copper and bcc iron. *Phil. Mag.* A **80**, 2131–2157.

Osetsky, Yu. N., Bacon, D. J., Serra, A., Singh, B. N. & Golubov, S. I. 2000*b* Stability and mobility of defect clusters and dislocation loops in metals. *J. Nucl. Mater.* **276**, 65–77.

Peierls, R. 1940 The size of a dislocation. *Proc. Phys. Soc.* **52**, 34–37.

Pelfort, M., Osetsky, Yu. N. & Serra, A. 2001 Vacancy interaction with glissile interstitial clusters in bcc metals. *Phil. Mag. Lett.* **81**, 803–811.

Puigvi, M. A., Osetsky, Yu. N. & Serra, A. 2003 Point-defect clusters and dislocation loops in bcc metals: continuum and atomistic study. *Phil. Mag.* **83**, 857–871.

Soneda, N. & Diaz de la Rubia, T. 2002 Migration kinetics of the self-interstitial atom and its clusters in bcc Fe. *Phil. Mag.* A **81**, 331–343.

Trinkaus, H., Heinisch, H. L., Barashev, A. V., Golubov, S. I. & Singh, B. N. 2002 1D to 3D diffusion-reaction kinetics of defects in crystals. *Phys. Rev.* B **66**, 060 105(R).

Trinkaus, H., Singh, B. N. & Foreman, A. J. E. 1992 Glide of interstitial loops produced under cascade damage conditions: possible effects on void formation. *J. Nucl. Mater.* **199**, 1–5.

Wirth, B. D., Odette, G. R., Maroudas, D. & Lucas, G. E. 1997 Energetics of formation and migration of self-interstitials and self-interstitial clusters in α-iron. *J. Nucl. Mater.* **244**, 185–194.

Woo, C. H. & Singh, B. N. 1990 The concept of production bias and its possible role in defect accumulation under cascade damage conditions. *Phys. Stat. Sol.* b **159**, 609–616.

Yoshiie, T., Ishizaki, T., Xu, Q., Satoh, Y. & Kiritani, M. 2002 One dimensional motion of interstitial clusters and void growth in Ni and Ni alloys. *J. Nucl. Mater.* **307–311**, 924–929.